

Theory and simulation of the dynamic heat capacity of the east Ising model

Jonathan R. Brown,^{1,2} John D. McCoy,^{1,a)} and Brian Borchers²¹Department of Materials and Metallurgical Engineering, New Mexico Institute of Mining and Technology, Socorro, New Mexico 87801, USA²Department of Mathematics, New Mexico Institute of Mining and Technology, Socorro, New Mexico 87801, USA

(Received 13 April 2010; accepted 30 June 2010; published online 13 August 2010)

A recently developed methodology for the calculation of the dynamic heat capacity from simulation is applied to the east Ising model. Results show stretched exponential relaxation with the stretching exponent, β , decreasing with decreasing temperature. For low temperatures, the logarithm of the relaxation time is approximately proportional to the inverse of the temperature squared, which is the theoretical limiting behavior predicted by theories of facilitated dynamics. In addition, an analytical approach is employed where the overall relaxation is a composite of relaxation processes of subdomains, each with their own characteristic time. Using a Markov chain method, these times are computed both numerically and in closed form. The Markov chain results are seen to match the simulations at low temperatures and high frequencies. The dynamics of the east model are tracked very well by this analytic procedure, and it is possible to associate features of the spectrum of the dynamic heat capacity with specific domain relaxation events. © 2010 American Institute of Physics. [doi:10.1063/1.3469767]

I. INTRODUCTION

Although “collective” or “cooperative” viscoelastic behavior evokes images of the migration of large groups of molecules *en masse*, in practice, such terms are typically applied to the movement of a material *en bulk* without explicit reference to its atomic nature. The descriptive language for the bulk behavior originates in the study of simple relaxation experiments. In particular, the analysis of a generic relaxation function, $x(t)$, usually involves a fit to the Kohlrausch–Williams–Watts¹ (KWW) (or, stretched exponential) function,

$$x(t) \propto \exp\left[-\left(\frac{t}{\tau}\right)^\beta\right], \quad (1.1)$$

where τ is the relaxation time and β is the “stretching exponent.” If the relaxation of the bulk system resulted from many isolated and identical activated processes, β would be unity and the function is said to be a Debye relaxation. Values of $\beta \neq 1$ are cited as evidence of “cooperatively;” however, because a direct probe of multiparticle cooperation is not involved, a better expression is a “non-Debye” relaxation. For fragile glass formers such as natural rubber or glycerol, β is less than 0.5 while for strong glass formers such as most inorganic glasses, β is close to the Debye limit.

Evidence of non-Debye behavior is seen in response experiments, and the dynamic heat capacity, the subject of the present study, is one of many such response functions. This approach was first pioneered experimentally by Birge and Nagel² and Christensen³ and showed similar behavior to other response functions.² The dynamic heat capacity is the response function resulting from imposing a sinusoidal tem-

perature “strain” on a material and tracking the energy of the system as a function of time. The phase lag of the energy permits the heat capacity to be expressed as in-phase (storage) and out-of-phase (loss) contributions. The loss frequency spectrum shows non-Debye behavior in the broadness of the low frequency, α -peak. Such response functions can also be found from the one-sided Fourier transform of the derivative of the appropriate relaxation functions. An α -peak corresponding to a Debye relaxation function is sharp and narrow and such $\beta=1$ behavior is rarely observed in any but the most molecularly simple glasses.

Usually response functions are fit directly in the frequency-domain by, for instance, the Cole–Davidson (CD) function,⁴ which, although not the transform of the KWW function, is of similar form. The CD function is given by

$$\chi(\omega) = \left(\frac{1}{1 + i\omega\tau}\right)^\beta = \cos(\beta\theta)\cos^\beta(\theta) - i \sin(\beta\theta)\cos^\beta(\theta), \quad (1.2)$$

where $\chi(\omega)$ is a response function, $i = \sqrt{-1}$, ω is frequency, and $\theta = \arctan(\omega\tau)$. The β and τ play the same role as their KWW counterparts, although they do not have the same values. Conversion relations between CD and KWW parameters exist,^{5,6} and $\beta=1$ reduces to the Debye case in both cases. A more general form is the Havriliak–Negami function,⁷

$$\chi(\omega) = \left(\frac{1}{1 + (i\omega\tau)^\alpha}\right)^\gamma, \quad (1.3)$$

where γ times α is similar to β and $\gamma = \alpha = 1$ is the Debye limit.

Finally, the non-Debye nature of the response functions of fragile glass formers is clearly seen by plotting storage versus loss moduli in a “Cole–Cole” plot. A Debye response

^{a)}Electronic mail: mccoy@nmt.edu.

function in a Cole–Cole plot is a semicircle while a CD function is flattened and distorted. Because time (or frequency) is not directly plotted in a Cole–Cole graph, such graphs are sensitive probes of the degree to which time-temperature superposition holds. Time-temperature superposition predicts Cole–Cole plots to be identical at all temperatures.

An advantageous aspect of simulation is the ability to work with simplified models which reduce the β -peak features while retaining the α -peak behavior. A model of extreme simplicity is the east model. This is a spin model and, as such, does not have many of the dynamical features commonly used to track the onset of glassy behavior such as diffusion and viscosity. On the other hand, it does capture the KWW behavior of fragile glass formers. A recently developed simulation methodology⁸ for computing the dynamic heat capacity is particularly well suited for the analysis of the east model.

A promising theory linking molecular details to non-Debye behavior is “facilitated dynamics.” In this perspective, motion is restricted by kinetic constraints or “defects” which can only be removed by defect-defect collisions. Highly simplified Ising models have succeeded in modeling such kinetic defects, and the east model is one of the best known of these. The east model shows rapidly increasing relaxation times as temperature is reduced and, importantly, its relaxation functions are non-Debye.

In the current study, we will show that the dynamic heat capacity of the east model displays clear evidence of non-Debye behavior and that the relaxation time defined by the α -peak rapidly increases with decreasing temperature. In addition, we present an algebraic solution of the dynamic heat capacity that is accurate at low temperature. Finally, we propose an extrapolation of the algebraic result that agrees well with the simulation results for a broad range of temperature.

II. GENERAL PROPERTIES OF THE EAST MODEL

The east model⁹ is a variant of the one dimensional Ising model, but with kinetic constraints. The Ising model has “spins” σ_i of 1 or 0, and the Hamiltonian is simply $\sum \sigma_i$. The equilibrium solution of this model is trivial. The probability, p , of a spin being +1 is

$$p = \exp\left(-\frac{1}{T}\right) \quad (2.1)$$

where T is the temperature and p is referred to as the “flip probability.” The concentration of up-spins, c , is

$$c = \frac{p}{p+1} = \frac{1}{1+\exp(1/T)} \quad (2.2)$$

and if the energy of the all-down-spin state is used as the zero of energy, c is also the average energy per spin. The constant volume heat capacity per spin, C_V , is then

$$C_V = \frac{1}{T^2} \frac{\exp(1/T)}{[1+\exp(1/T)]^2}. \quad (2.3)$$

What makes this model of interest is the manner in which dynamics are incorporated. Spins can only flip if they are “released” at which time they flip according to the usual Metropolis Monte Carlo (MC) rules. Each pass through the released spins counts as a single timestep. In the east model, a spin can only flip if the spin to its right (i.e., the east) is in the up-state.

Consider what happens at low temperature where the concentration of up-spins is small. An up-spin is essentially trapped in the up position because the spin to its right is almost certainly down, but, on the other hand, the spin to its left is released and can flip up. When this spin flips up it releases the spin to its left, etc. Consequently, the system is split into domains separated by up-spins with a fair amount of motion to the up-spin’s left, but little to its right. The rapid left-side motion is local and would contribute to high frequency, β -peaks in the loss spectra. The slow motion corresponding to the low frequency, α -relaxation is the release of the domain-dividing, up-spins. The release of one of these spins is only possible when an up-spin works its way gradually from the next up-spin to the right. This, of course, is the result of a long sequence of β -relaxations.

The idea that α -relaxations result from a sequence of β -relaxations is not new, and the east model intentionally builds in this physics. The interesting aspect of the model is that the relaxation functions resulting from this model are of the KWW type. Moreover, α -relaxations are the result of defect pairs (an up-spin to the left that will move and an up-spin to the right that generates a β -event chain to the left in order to release the other up-spin). As a result, the relaxation time, τ , is expected¹⁰⁻¹³ to vary as an exponential inverse temperature squared (EITS) function of relaxation time,

$$\tau \propto \exp\left[\frac{B}{T^2}\right], \quad (2.4)$$

where B is a model specific constant. Aldous and Diaconis¹⁰ reported bounds on B for the east model of $1/(2 \ln 2) \leq B \leq 1/\ln 2$. Sollich and Evans^{11,12} reported B to be $1/\ln 2$ although this was not a rigorous argument.^{10,13} Finally, Cancrini *et al.*¹³ reported B to be $1/2 \ln 2$ in the low temperature limit.

III. METHODOLOGY

We use two methods to explore the dynamic heat capacity of the east model. First, we apply a simulation technique⁸ developed for the study of bead-spring glasses. Second, we develop a Markov chain model of cascades of β -events over the up-spin separated domains. This second approach is approximate because of the necessity of the truncation of a series expansion; however, it provides an excellent explanation of the β -peaks in the loss modulus of the dynamic heat capacity. In this section we discuss these two methodologies.

The simulation itself is a straightforward application of the rules of the east model. A random starting configuration was chosen for all the spins with the correct concentration of up-spins by setting each site to be up or down with probability “ c ” of being up. “Time” was then iterated with time re-

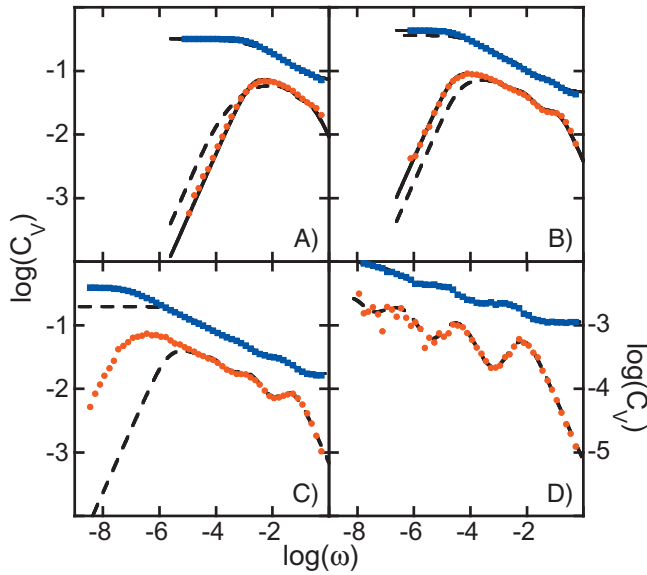


FIG. 1. Real and imaginary components of the dynamic heat capacity plotted against frequency on a log-log scale for a range of temperatures. The squares and circles are the real and imaginary parts of the simulation data, respectively, with every other point dropped for clarity. The dashed line is the Markov chain Debye series computation, truncated by the number of terms that could be computed numerically. The solid line is the extended Markov chain Debye series fit. The parameters for the four plots are (a) a temperature of $T=0.7$, domain length at truncation $d_{\text{trunc}}=20$, and best fit maximum effective domain length $d_{\text{max}}=6$; (b) $T=0.45$, $d_{\text{trunc}}=17$, and $d_{\text{max}}=14$; (c) $T=0.32$, $d_{\text{trunc}}=16$, and no possible fit for d_{max} ; (d) $T=0.2$, $d_{\text{trunc}}=14$, and no possible fit for d_{max} .

ported in units of Monte Carlo steps. At each step, the temperature was recomputed to follow a sinusoidal form $T(t) = T_0 + \Delta T \sin(\omega t)$, and, in particular, the flip probability p was evaluated. The state of the system (step number, temperature, and average energy per site) was dumped at regular intervals and saved for postprocessing.

The Monte Carlo scheme was run for a range of 40 temperatures between 0.2 and 10, and, for each temperature, numerous runs of logarithmically spaced periods were performed. In particular, 12 periods were selected per order of magnitude, and the periods ranging from 10 to a value large enough to reach, if possible, the low frequency limiting behavior. Computational limitations restricted the maximum period to be at most 10^9 . From this we are able to compute a dynamic heat capacity spectrum during post processing following the methodology outlined in our previous study.⁸ In brief, in the linear response regime and at each frequency, the energy will have an amplitude ΔE and phase lag δ . The dynamic heat capacity $C = C' + iC''$ is then given by

$$C'(\omega) = \frac{\Delta E}{\Delta T} \cos(\delta), \quad C''(\omega) = \frac{\Delta E}{\Delta T} \sin(\delta). \quad (3.1)$$

The amplitude of oscillations used was $\Delta T = 0.05T_0$, and the number of sites used was $N = 100\,000$ for most temperatures and $N = 200\,000$ for the colder temperatures, where the average energy per spin becomes small. In order to check that the results were not an anomaly of these chosen parameters, both ΔT and N were varied for a limited range of temperatures.

Typical results are shown in Fig. 1. Temperatures are

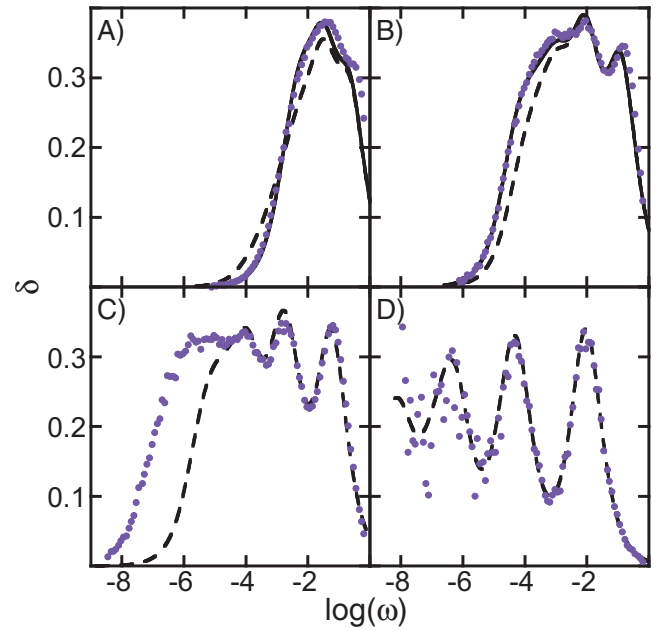


FIG. 2. The phase lag δ plotted against frequency on a semilogarithmic scale for the same range of temperatures as Fig. 1. The circles are the simulation data and the lines have the same meaning as in Fig. 1.

0.7, 0.45, 0.32, and 0.2; the upper curve in each panel is the storage modulus and the lower is the loss modulus. Strictly speaking, the equilibrium value of the heat capacity is at zero frequency where the loss modulus is zero and the storage modulus agrees with Eq. (2.3). In practice, the low frequency limit in our work corresponds to frequencies sufficiently low that the storage modulus displays a plateau with a value approximately equal to the equilibrium value of Eq. (2.3). In addition, the loss modulus in this limit has a well defined power law behavior with a power of about 1. In Fig. 1, panels (a), (b), and (c) corresponding to temperatures 0.7, 0.45, and 0.32, respectively, are seen to reach the equilibrium limit while panel (d) for $T=0.2$ does not. It is worth noting that the high frequency results in Fig. 1(d) are accurate representations of the β -relaxation behavior of the system.

The general features of the moduli are as expected. The low frequency, α -peak in the loss modulus is seen to shift to lower frequencies (i.e., longer relaxation times) as the temperature is lowered. Interestingly, although the systems show a well defined rubbery plateau at low frequencies, a glassy plateau is not seen. One might expect that a glassy plateau would appear at even higher frequency; however, the east model has an inherent upper cutoff in frequency corresponding to a single Monte Carlo timestep. Finally, the loss modulus is seen to develop a well defined power law region on the high frequency side of the α -peak. Once fully developed, the slope of this region is roughly -0.2 which is indicative of non-Debye behavior (Debye behavior would imply a slope of -1 in this region). For the CD function, this slope corresponds to $-\beta$, resulting in $\beta_{\text{CD}} = 0.2$. In Fig. 2, the phase lag, δ , is plotted for the same systems shown in Fig. 1. Viewed in this manner, the β -peaks are quite pronounced, and the non-Debye power law region is manifested as a plateau clearly seen in Fig. 2(c).

The same results are plotted in the Cole-Cole form in

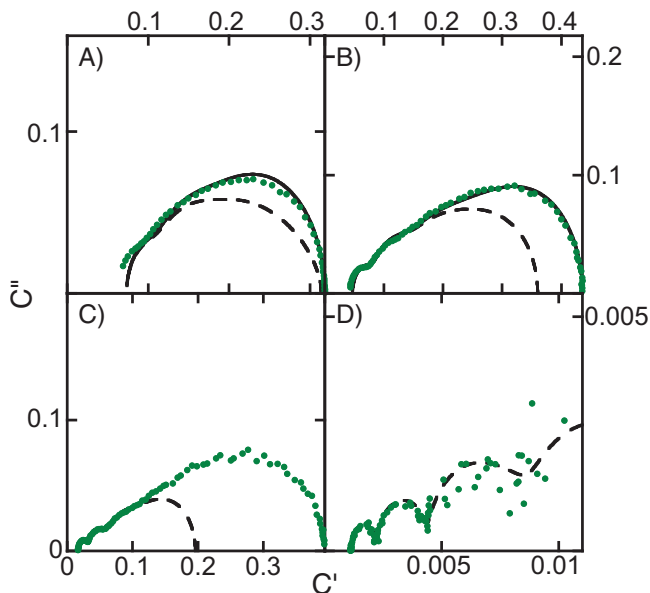


FIG. 3. Cole-Cole plots for the same range of temperatures as Fig. 1. The circles are the simulation data and the lines have the same meaning as in Fig. 1. The range of the real axis in plots (a)–(c) is between zero and the equilibrium heat capacity. The scale on the imaginary axis is twice the scale on the real axis for clarity.

Fig. 3. The noncircular, non-Debye nature of the dynamic heat capacity is apparent. The CD value of β can be found following Davidson's method⁴ where the slope of the Cole-Cole plot at high frequency (or small loss modulus) is set equal to $\beta\pi/2$. The slope is 0.3 in Fig. 3(c) resulting in a $\beta_{CD}=0.2$ in agreement with the β found from the slope of the loss modulus in Fig. 1(c). The corresponding KWW β is approximated⁶ through the relation $\beta_{KWW}=0.970\beta_{CD}+0.144$ to be $\beta_{KWW}=0.35$.

In order to fit the simulations to phenomenological functions in more detail, the Havriliak-Negami (HN) function was employed along with a frequency-domain approximation of the KWW function due to Bergman.¹⁴ As in the discussion above, the data have high frequency β -peak structures which cannot be fit with HN or KWW expressions. In order to fit the data in a reasonable manner, the β -peak region is not included in the curve fits. For example, for the system shown in Fig. 1(c), the data for frequencies above $\log(\omega) \sim -4$ were not included.

The other method that we used predicts the form of the modulus from analytic arguments and, consequently, has more explanatory power. The system is treated as a series of domains of down-spins with an up-spin on either side. This is the approach proposed by Sollich and Evans^{11,12} that was used to predict that the logarithm of the relaxation time grows proportionally to the inverse of the temperature squared. We expand on their approach and compare the resulting dynamic heat capacity to simulation. The interested reader is referred to the more sophisticated analysis of the methodology in the original papers.^{11,12}

Each domain length will have a specific relaxation time associated with it. This is the mean first passage time when the right hand up-spin and all intermediate spins are flipped down. This is found with a Markov chain analysis as follows.

Fix a domain of length d , and let \mathbf{P} be the transition matrix, where we have assumed that there is an up-spin to the left of the domain that does not relax and we use the convention that P_{ij} is the probability that state i transitions to state j . This matrix is $2^d \times 2^d$ and sparse since each row can have only as many as $2^{d/2}$ nonzero elements, and typically much less. If state j can follow from state i in a single step, this probability is nonzero and can be written as $P_{ij}=p^{u(i,j)}(1-p)^{v(i,j)}$, where $u(i,j)$ is the number of sites that need to flip up for the system to go from state i to state j , and $v(i,j)$ is the number of sites that could flip up but does not in the transition.

To measure the mean first passage time in question, we make the relaxed state of the system an absorbing state and calculate the mean absorbing time. Since there is a fixed up-spin to the left of the domain, it is easy to see that any configuration can be reached from any other configuration with nonzero probability given enough steps, so the original chain is ergodic.¹⁵ This would make the relaxed state the only absorbing state and connected to all the transient states.

The mean absorption time is found from solving the system of equations,¹⁵

$$(\mathbf{I} - \mathbf{Q})\underline{\tau} = \underline{v}, \quad (3.2)$$

where \mathbf{I} is the identity matrix, \mathbf{Q} is the part of the matrix \mathbf{P} with the row and column associated with the absorbing state removed, \underline{v} is a vector of all ones, and $\underline{\tau}$ is the vector of mean absorption times for each starting state. The relaxation time of the domain τ_d is the element of $\underline{\tau}$ that corresponds to the unrelaxed state.

By straightforward application of the rules of the east model, we can compute $(\mathbf{I} - \mathbf{Q})$ for relatively small values of domain length d . By the symbolic computation toolbox in MATLAB,¹⁶ the mean passage time was computed as above for an arbitrary temperature. Since it is computationally intensive to solve large symbolic systems, the same problem was also solved numerically at the specific temperatures that were run in the MC simulations. For small length chains, this was done directly, but for larger chains this was done with the GMRES iterative solver¹⁷ up to an accuracy of 10^{-3} or better. The $\mathbf{I} - \mathbf{Q}$ matrices are generally ill conditioned so a Jacobi preconditioner was used to speed up the iterative solver.

Next, under the approximation that the up-spins are isolated enough that the up-spin on the left hand side of the domain does not relax, we can treat the system as if it were a population of independent domains. Let $N(d)$ be the number of sites of length d . In equilibrium, each orientation of spins is equally likely so the length of domains follows a geometric distribution,

$$N_{eq}(d) = Nc(1-c)^{d-1}. \quad (3.3)$$

In the time domain, the equivalent to the dynamic heat capacity is the average fluctuations of the energy from equilibrium, ΔE . Focusing on a single domain length d the contribution to ΔE is just $\Delta N(d) = N(d) - N_{eq}(d)$. The mean time for a domain to relax is τ_d , and since the time rate of change of the number of domains is proportional to how many such domains there are, we can reasonably model this with the

Debye relaxation for domains of at least size two. For the $d=1$ case, the relaxation always happens in a single step, so there is no imaginary/loss part to it. Also, for the $d=2$ case, the relaxation happens in exactly two steps with probability p so there is no loss part in this case either. The individual Debye forms are weighted by how many domains there should be in equilibrium. That is, the dynamic heat capacity is a summation in domain length of Debye relaxations with each term weighted by Eq. (3.3). Specifically,

$$C_V(\omega) = C_V \left[c + c(1-c) \left(p + \frac{(1-p)}{1+i\omega\tau_2} \right) + \sum_{d=3}^{\infty} \frac{c(1-c)^{d-1}}{1+i\omega\tau_d} \right]. \quad (3.4)$$

Equation (3.4) has the advantage of being based only on numerically accurate calculations instead of fitting parameters, but its weakness is that it ignores domain-domain interactions. Again drawing on the results of Sollich and Evans,¹² large domains relax as a result of a moving “front” of up-spins from the left. This happens because domains that are long enough to relax slower than their neighbor, on average, will be necessarily nonisolated. Therefore, the far left up-spin will tend to be relaxed by the adjacent domain; this will often have the effect of shrinking the domain in question because it will likely have flipped up an intermediate spin, which will become the new terminal left spin for the domain, which is now more stuck. The details are complicated, but we can modify Eq. (3.4) to incorporate this effect by adding the fitting parameter d_{\max} , the maximum isolated domain length. From Fig. 3 of Ref. 12, the relaxation time of very long (that is, nonisolated) domains is seen to vary linearly with domain length, as one would expect from a fixed velocity front of up-spins. That is, for $d > d_{\max}$,

$$\tau_d = \frac{\tau_{\max}}{d_{\max}} d. \quad (3.5)$$

We will refer to Eq. (3.4) as the Markov chain Debye series model, and the modification in Eq. (3.5) as the extended Markov chain Debye series model.

IV. RESULTS

The result of the symbolic computation of the domain relaxation times was

$$\tau_1 = 1,$$

$$\tau_2 = p^{-1} + 1,$$

$$\tau_3 = \frac{p^3 - 2p - 1}{p^2(1-p)} = p^{-2} + 3p^{-1} + 3 + O(p),$$

$$\tau_4 = 2p^{-2} + 4p^{-1} + 4 + O(p),$$

$$\tau_5 = \frac{1}{2}p^{-3} + \frac{15}{4}p^{-2} + \frac{71}{8}p^{-1} + \frac{163}{16} + O(p),$$

$$\tau_6 = \frac{6}{7}p^{-3} + \frac{37}{7}p^{-2} + \frac{90}{7}p^{-1} + \frac{818}{49} + O(p),$$

$$\tau_7 = \frac{3}{2}p^{-3} + \frac{27}{4}p^{-2} + \frac{289}{12}p^{-1} + \frac{751}{144} + O(p),$$

$$\tau_8 = 4p^{-3} - 40p^{-2} + \frac{2509}{2}p^{-1} - \frac{477\,655}{16} + O(p). \quad (4.1)$$

The symbolic computation could not be performed in a reasonable amount of time for domain sizes larger than $d=8$. These expressions for domain relaxation times are in agreement with the prediction of Sollich and Evans that $\tau_d = p^{-n}$ to leading order for small p , where $2^{n-1} < d \leq 2^n$. Also, a similar computation shows that in the isolated case the creation time for domains $\tau_d^* = \tau_d/p$.

Figures 1–3 show the dynamic heat capacities computed from simulation compared to the models from the previous section for four temperatures picked to exemplify the full range of temperatures that were probed. The Markov chain Debye series fits the simulation data reasonably well for high frequencies at all temperatures, but for low temperatures, where relaxation times are large and the exponential approximation is very good, the model matches the data extremely well [see panels (c) and (d) in Figs. 1–3]. This model does not fit very well for low frequencies, nor do we expect it to because low frequencies correspond to large relaxation times and large domains, which are more likely to be nonisolated and relax more quickly [see panel (a) of Figs. 1–3]. The extended Markov chain Debye series model matches the simulation data more closely [see panels (a) and (b) in Figs. 1–3]. The parameter d_{\max} was fit for 13 temperatures between 0.42 and 1.0 (where such a fit was possible) and scales linearly with the mean domain size $\langle d \rangle$ obeying the relationship $d_{\max} = 1.6\langle d \rangle - 2.2$ [see Fig. 4(c)]. The relaxation time of the maximum isolated domain τ_{\max} scales roughly linearly with the overall relaxation time [see Fig. 4(d)]. Both models suffer from increasing difficulty in computing relaxation times, as each term is, in general, four times harder than the previous term to compute, and the matrices become increasingly ill conditioned for lower temperatures [see panels (b) and (c) of Figs. 1–3].

For many experimental systems, it is often assumed that the functional form of the response and relaxation functions does not change appreciably with temperature beyond the variation in τ . If this is the case, one would expect the moduli to superimpose, or, in other words, expect that time-temperature superposition would be obeyed. In Fig. 4(a), the loss modulus at a number of different temperatures is plotted with the frequency axis normalized by the frequency at the maximum, ω_p , and the modulus normalized by its magnitude at the maximum. We see the difficulty in determining if time-temperature superposition is obeyed or not. At low frequency, the curves superimpose very well, as they do near the maximum. On the high frequency side, however, the curves do not superimpose. On the other hand, this is the region where β -relaxations are prevalent and time-temperature superposition is not expected to work for β -peaks. It should be noticed that the curves appear to be

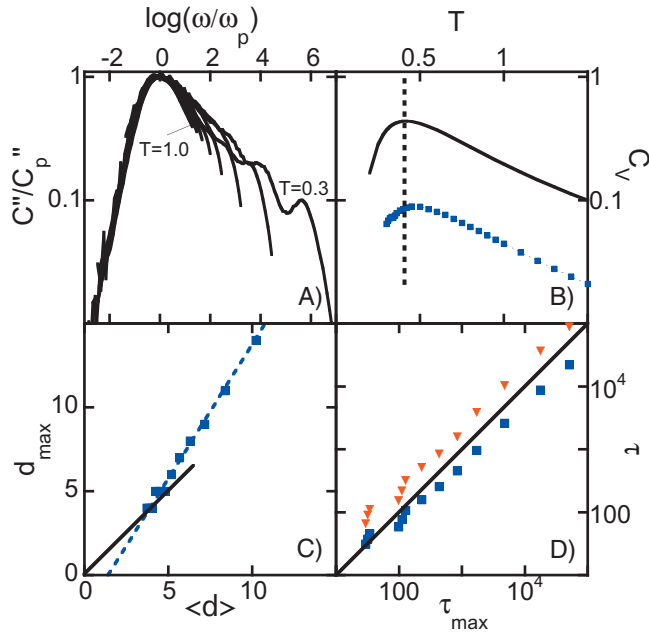


FIG. 4. (a) The imaginary part of the dynamic heat capacity normalized by peak height plotted against frequency normalized by peak frequency on a log-log scale. Each curve is from simulation data for temperatures ranging from $T=0.3$ to $T=1.0$ (as labeled), and each successive curve differs from the next by a constant change in temperature of 0.1. (b) Equilibrium heat capacity (solid line) and imaginary peak height from simulation (squares) plotted against temperature. The vertical dashed line goes through the peak of the equilibrium heat capacity. (c) Fitted maximum isolated domain length d_{\max} plotted against the mean domain length $\langle d \rangle$. The solid line has a slope of one, and the dashed line is a linear fit to the data. (d) Relaxation time τ for the KWW (squares) and HN (inverted triangles) fits plotted against the relaxation time of the largest nonisolated domain τ_{\max} on a log-log scale. The solid line has a slope of one.

approaching a high frequency limit of a straight line with slope of -0.2 . Consequently, it is reasonable to believe that the response function for the system is composed of an α -peak contribution with a $\beta_{CD}=0.2$ and a series of β -peaks where the α -peak obeys time-temperature superposition and the β -peaks do not.

The height of the imaginary peak is of interest because it is proportional to the maximum amount of entropy generated per cycle.⁸ The peak height of the loss modulus and the equilibrium heat capacity are plotted against temperature in Fig. 4(b). The vertical line emphasized the difference in the maxima between the two; the heat capacity has a maximum at $T=0.42$ and the maximum peak height is at about $T=0.45$.

Finally, in Fig. 5, the parameters from the HN and KWW fits are plotted. The relaxation time τ calculated from the HN fit differs slightly from that calculated from the KWW fit. This is to be expected because the two relaxation times measure slightly different aspects of the spectra; however, they have a similar temperature dependence. Part A of this plot shows the relaxation times for KWW fit to a Vogel-Fulcher form,¹⁸

$$\tau = \tau_0 \exp \left[\frac{A}{(T - T_0)} \right], \quad (4.2)$$

where τ_0 , A , and T_0 are fitting parameters. This fitting procedure predicts a divergence at $T_0=0.15$ [this fit is shown in

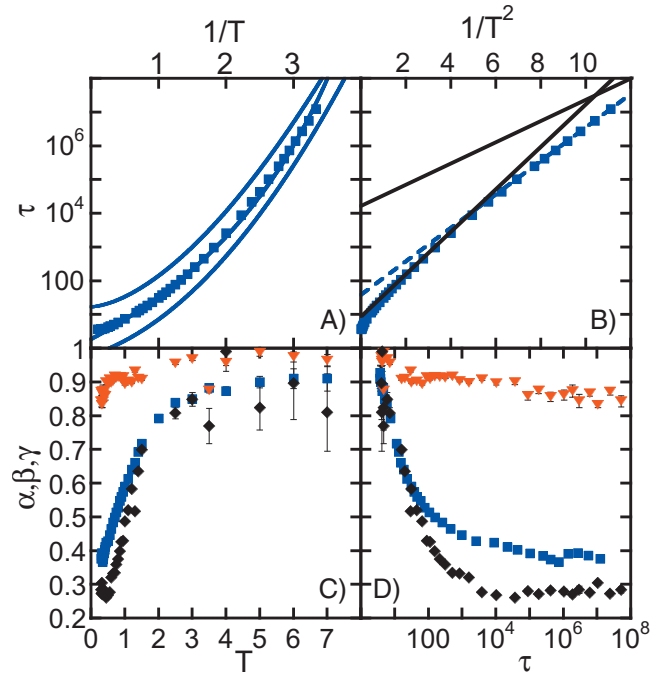


FIG. 5. Plots of the fitting parameters. (a) Relaxation time τ plotted against inverse temperature on a semilogarithmic scale. The squares are from KWW fits to simulation data. The center curve is a Vogel-Fulcher fit, the upper curve fit is to $\ln(\tau) \sim 1/T^\delta$ with $\delta=1.63$, the lower curve fit is to $\ln(\tau) \sim ((1/T) - (1/T_0))^2$ with $T_0=-1.254$. Upper and lower curves are shifted vertically for clarity. (b) Relaxation time plotted against inverse temperature squared on a semilogarithmic scale. The squares are from KWW fits to the simulation data. The dashed line is an EITS fit to the last six relaxation times. The solid lines have slopes of $1/\ln 2$ and $1/2 \ln 2$. (c) Shape parameters fit from simulation data, β (squares) α (inverted triangles), and γ (diamonds), plotted against temperature. (d) Shape parameters plotted against relaxation time on a semilogarithmic scale.

the central curve of Fig. 5(a)]; however, because the detailed nature of the model dynamics is so transparent, it is difficult to conceive of a true divergence at a nonzero temperature. The flip probability is well defined in this model and is simply related to the temperature. As long as there is motion (i.e., spin flips), up-spins will be able to propagate and relax the system. Indeed, the east model has been shown to be ergodic^{10,13} at all temperatures. Of course, this is not to say that other more complex glass formers do not diverge at finite temperature.

In Fig. 5(b), the relaxation time is plotted as suggested by Eq. (2.4), where τ is expected to be an exponential function of inverse temperature squared. Although the curve is not linear over its entire range, it does have an extended linear region at low temperature. The slope, B , of this linear region is in the range between $1/\ln 2$ and $1/(2 \ln 2)$ as predicted by Sollich and Evans,^{11,12} Aldous and Diaconis,¹⁰ and Cancrini *et al.*¹³ For the HN fits (not shown) this results in $\tau_0=171.47$ and $B=1.136=0.787/\ln 2$, and for KWW $\tau_0=38.094$ and $B=1.1425=0.792/\ln 2$.

The variation in the “shape” parameters from the HN and KWW fits are shown in Figs. 5(c) and 5(d). Recall that α times γ from the HN fit is approximately β_{CD} and that β_{CD} can be related to β_{KWW} through the Lindsey-Patterson curve fit.⁶ For instance, in the large relaxation time limit in Fig. 5(d), the HN fit gives $\alpha=0.29$ and $\gamma=0.85$ which implies that

$\beta_{CD}=0.25$ and, consequently, that $\beta_{KWW}=0.39$. This is in agreement with the direct KWW fit shown in the figure. If we assume that β_{KWW} is linear with temperature at low temperature, then the $T=0$ limit is $\beta_{KWW}=0.25$, although the lowest value of β_{KWW} found in our study was roughly 0.35. A conservative estimate of the $T=0$ limit for the east model would be $\beta_{KWW}=0.3 \pm 0.05$.

V. DISCUSSION

Typically, the analysis of the onset of glassy behavior focuses on (1) the temperature dependence of the characteristic relaxation time and (2) the functional form of the relaxation or response function. Here, we discuss the implications of our work in these areas and compare with similar studies of others. Finally, we briefly summarize the results.

If the relaxation process was the result of a cascade of activated processes, the relaxation time would be given by an Arrhenius form, $\tau \sim \exp[E_T/T]$, where E_T is an activation energy. This perspective has a long history of use^{19–21} where different temperature dependencies of E_T are used to fit experiment. A form accurate for temperatures below the “mode coupling temperature,” T_C , is

$$\tau \sim \exp[C((T_C/T) - 1)^2]. \quad (5.1)$$

On the other hand, for temperatures above T_C , power law behavior, $\tau \sim (T - T_C)^{-\gamma}$, is typically seen where γ should not be confused with the HN γ . For the east model, Fig. 5(b) suggests that the T_C occurs at the deviation from linear behavior which (roughly $T=0.5$), and that γ is 1.7. This can be compared to polystyrene²⁰ where $\gamma=3.45$, $T_C=445$ K, and the experimental glass transition temperature T_g is 384 K; to bead-spring chains²² where $\gamma \sim 2$. Switching between power law at high temperature and $E_T \sim 1/T$, activated process at low temperature works well to explain the behavior of many systems^{20,23} (e.g., see Fig. 15 of Ref. 23). Recent work²⁴ has used a low temperature, activated process picture to fit a wide range of experimental results.

Our results can be fit with Eq. (5.1) yielding $C=0.597$ and $T_C=-1.254$ [the lower curve in Fig. 5(a)]. Notice that CT_C^2 can be interpreted as a fit of B from Eq. (2.4), resulting in $B=0.938=0.650/\ln 2$ which is close to the limit of $1/2 \ln 2$. On the other hand, T_C is negative and would not correspond to a thermodynamically accessible temperature. A reasonable explanation of the accuracy of Eq. (5.1) for the east model is as an average over relaxation mechanisms. In the high temperature limit, all domains are nonisolated so a domain’s relaxation time is directly proportional to its length. This implies that the mean relaxation time is proportional to the mean domain length, or $\tau \sim \exp(1/T)$ at large T while $\tau \sim \exp(1/T^2)$ at low T . The function $\tau \sim \exp[(A/T)^2 + (B/T)]$ is equivalent to Eq. (5.1) and is an interpolation between the two temperature extremes. In addition, we can fit the relaxation time across the entire temperature range with a general power law in inverse temperature, $\tau \sim \exp[C(1/T)^\delta]$. This fit is shown as the upper curve in Fig. 5(a) and it yields an exponent of $\delta=1.63$.

We now turn our attention to the functional form of the response function. Several dynamic heat capacity simulation

studies have previously been done on glass forming models. A typical result shows the imaginary part of the spectrum to have two peaks, corresponding to α and β processes. Often the α -peak has a stretched, Cole–Davidson shape to it, and the β -peak is typically about ten times the height of the α -peak. Such behavior is seen in a variety of molecular models, for example, in molecular dynamics studies by Grest and Nagel²⁵ on a binary Lennard-Jones mixture with parameters selected to model glycerol (see Fig. 6 of Ref. 25, the α -peak is at lower frequencies than probed), by Scheidler *et al.*²⁶ on a binary Buckingham plus Columbic mixture with parameters selected for silica (see Fig. 3 of Ref. 26), and by Brown *et al.*⁸ on a bead-spring polymer (see Fig. 2 of Ref. 8). It is also observed in an energy landscape inspired model by Chakrabarti and Bagchi²⁷ where a number of two-level systems are coupled together.

Unlike the atomically detailed models and the energy landscape model, there are no inherently local (e.g., vibrational) β processes in the east model. Instead, the high frequency/short time peaks are a result of short time processes on isolated short domains separated from the long time processes associated with the long domains. In both the molecular models and energy landscape models, the β -processes contribute about ten times as much to the overall heat capacity as the cooperative processes do; in the east model, however, all of the thermodynamics is a result of cooperation. The relaxation of large domains requires the creation/destruction of many smaller intermediate domains on much shorter timescales, so, in that sense, α relaxation is a result of a large local collection of “ β ” excitations for all of the models discussed. However, the β processes of the east model are intimately tied to the stretching of the α process, whereas in the other models discussed the β processes are fundamental short time interactions which may or may not be closely associated with the α process.

Other simulation studies have investigated relaxation functions of the east model in the time domain. Fitting to a KWW form is necessarily a crude approximation at short times for any facilitated spin model because the dynamics are inherently discrete. It is, however, a good approximation for longer times, and finding a theoretical basis for the KWW form was one of the early justifications of such models.²⁸ The initial paper⁹ on the east model fits to a KWW form and yields a $\beta_{KWW}=0.403$ for a numerical computation based on a chain length of $N=9$ and an average up-site concentration of $c=0.3$, corresponding to approximately $T=1.18$ in the present study. A study by Pitts *et al.*,²⁹ which also used the lattice gas definition of the model, predicts a $\beta_{KWW}=0.26$ (extracted from Fig. 2 of Ref. 29) for their coldest run with concentration of $c=0.05$ ($T=0.340$); this is derived from a Monte Carlo simulation with $N=1000$. Note that the “wiggles” that appear in the time-domain relaxation of cold systems (see Fig. 1 of Ref. 29) correspond to distinct high frequency peaks of the dynamic heat capacity [see Figs. 1(c) and 1(d)]. A study by Witkoskie and Cao³⁰ finds β ’s between 0.36 and 0.47 depending on how the fit was done for a system with $c=0.10$ ($T=0.455$); this is comparable to our value of $\beta=0.42$ for the KWW fit with $T=0.45$. They also measured domain lifetimes as a function of domain length, which

produces a function quite similar to the imaginary part of the dynamic heat capacity (see Fig. 6 of Ref. 30).

One could extend our work with more computational time and/or smarter solvers. That is, lower temperatures and larger domain relaxation times could be studied. However, this would take many additional orders of magnitude of computational time.

In summary, we have applied a recently developed methodology of driven temperature simulations to the east Ising model in order to better understand its dynamics. These dynamics were probed as a function of frequency and the results were in agreement with other studies: The α -peak is found to be non-Debye with a $\beta_{\text{KWW}} \sim 0.3$ at low temperature; the stretching exponent is found to decrease with decreasing temperature; increasingly pronounced β -structure is found as temperature decreases with multiple peaks extending to lower frequencies than found in less simple models such as bead-spring chains.

One of the most intriguing aspects of the east model is that its simplicity permits, to a degree, one to trace the β -events to the resulting α -behavior. We approached this goal by breaking the relaxation process into a series of domain relaxations and evaluating each domain relaxation in terms of its component spin flips. This Markov chain model resulted in an excellent explanation for the high frequency behavior seen in simulation at all temperatures. At high temperature the approach breaks down because of domain coupling. At low temperature the approach becomes impractical because of the computational demands. Finally, we introduced a low temperature approximation, the extended Markov chain method, which gave excellent agreement with simulation at high temperature across the full frequency range.

ACKNOWLEDGMENTS

The authors thank Lorie Liebrock and Brian Hughes for time on the Exemplar minisupercomputer at New Mexico Tech.

- ¹R. Kohlrausch, *Ann. Phys.* **91**, 56 (1854); G. Williams and D. C. Watts, *Trans. Faraday Soc.* **66**, 80 (1970).
- ²N. O. Birge and S. R. Nagel, *Phys. Rev. Lett.* **54**, 2674 (1985).
- ³T. Christensen, *J. Phys. Colloq.* **46**, 635 (1985).
- ⁴D. Davidson and R. Cole, *J. Chem. Phys.* **19**, 1484 (1951); D. W. Davidson, *Can. J. Chem.* **39**, 571 (1961).
- ⁵T. C. Dotson, J. Budzien, J. D. McCoy, and D. B. Adolf, *J. Chem. Phys.* **130**, 024903 (2009).
- ⁶C. P. Lindsey and G. D. Patterson, *J. Chem. Phys.* **73**, 3348 (1980).
- ⁷S. Havriliak and S. Negami, *Polymer* **8**, 161 (1967).
- ⁸J. R. Brown, J. D. McCoy, and D. B. Adolf, *J. Chem. Phys.* **131**, 104507 (2009).
- ⁹J. Jäckle and S. Eisinger, *Z. Phys. B: Condens. Matter* **84**, 115 (1991).
- ¹⁰D. Aldous and P. Diaconis, *J. Stat. Phys.* **107**, 945 (2002).
- ¹¹P. Sollich and M. R. Evans, *Phys. Rev. Lett.* **83**, 3238 (1999).
- ¹²P. Sollich and M. Evans, *Phys. Rev. E* **68**, 031504 (2003).
- ¹³N. Cancrini, F. Martinelli, C. Roberto, and C. Toninelli, *Probab. Theory Relat. Fields* **140**, 459 (2008); *J. Stat. Mech.: Theory Exp.* **2007**, L03001.
- ¹⁴R. Bergman, *J. Appl. Phys.* **88**, 1356 (2000).
- ¹⁵J. G. Kemeny and J. L. Snell, *Finite Markov Chains* (Springer-Verlag, New York, 1976).
- ¹⁶MATLAB version 7.8.0, Natick, Massachusetts, The MathWorks Inc., 2010.
- ¹⁷Y. Saad and M. H. Schultz SIAM (Soc. Ind. Appl. Math.) *J. Sci. Stat. Comput.* **7**, 856869 (1986).
- ¹⁸H. Vogel, *Phys. Z.* **22**, 645 (1921); G. S. Fulcher, *J. Am. Ceram. Soc.* **8**, 339 (1925).
- ¹⁹T. G. Fox and J. P. Flory, *J. Am. Chem. Soc.* **70**, 2384 (1948).
- ²⁰R. Richert, and H. Bassler, *J. Phys.: Condens. Matter* **2**, 2273 (1990).
- ²¹J. D. Ferry, L. D. Grandine, and E. R. Fitzgerald, *J. Appl. Phys.* **24**, 911 (1953).
- ²²J. V. Heffernan, J. Budzien, A. T. Wilson, R. J. Baca, V. J. Aston, F. Avila, J. D. McCoy, and D. B. Adolf, *J. Chem. Phys.* **126**, 184904 (2007).
- ²³W. Gotze and L. Sjogren, *Rep. Prog. Phys.* **55**, 241 (1992).
- ²⁴Y. S. Elmatad, D. Chandler, and J. P. Garrahan, *J. Phys. Chem. B* **113**, 5563 (2009).
- ²⁵G. S. Grest and S. R. Nagel, *J. Phys. Chem.* **91**, 4916 (1987).
- ²⁶P. Scheidler, W. Kob, A. Latz, J. Horbach, and K. Binder, *Phys. Rev. B* **63**, 104204 (2001).
- ²⁷D. Chakrabarti and B. Bagchi, *J. Chem. Phys.* **122**, 014501 (2005).
- ²⁸R. G. Palmer, D. L. Stein, E. Abrahams, and P. W. Anderson, *Phys. Rev. Lett.* **53**, 958 (1984).
- ²⁹S. J. Pitts, T. Young, and H. C. Andersen, *J. Chem. Phys.* **113**, 8671 (2000).
- ³⁰J. B. Witkoskie and J. Cao, *Phys. Rev. E* **69**, 061108 (2004).